ELSEVIER

International Journal of Heat and Fluid Flow 19 (1998) 150–158

International Journal of HEAT AND FLUID FLOW

Pressure transport in direct numerical simulations of turbulent natural convection in horizontal fluid layers

Martin Wörner *, Günther Grötzbach

Research Centre Karlsruhe, Institute for Reactor Safety, P.O. Box 3640, 76021 Karlsruhe, Germany

Received 15 August 1997; accepted 25 October 1997

Abstract

Direct numerical simulation (DNS) data of two types of turbulent natural convection in horizontal fluid layers are used to compute turbulent diffusive transport terms for turbulence kinetic energy and vertical turbulent heat flux. For both quantities turbulent diffusive transport is represented by a pressure correlation and a triple correlation. While for Rayleigh–Bénard convection in air the pressure correlation dominates the triple correlation, for the convection in an internally heated layer the opposite behaviour is observed. The dominance of pressure transport in the Rayleigh–Bénard convection and its minor importance in the internally heated layer is explained by the coherent structures and dynamics of the respective flow. The coherent structures are intermittent; they exist only for limited time intervals. Thus, conventional closure relations for turbulent diffusive transport, which are used in statistical turbulence models basing on long-time averaged quantities, may not be appropriate for the flows under consideration.

Keywords: Pressure transport; Turbulent natural convection; Direct numerical simulation

Notation

Bo	Boussinesq number, $Pr^2\ Gr$
D	channel height
$D_{k,\mathrm{turb}}$	turbulent diffusion in k-equation
$D_{q_i,\mathrm{turb}}$	turbulent diffusion in q_i-equation
Da	Damköhler number, $q_v D^2/(\lambda\,\Delta T_{\max})$
g	gravitational acceleration
Gr	Grashof number, Ra_E/Pr
k	turbulence kinetic energy, $\overline{u_i' u_i'}/2$
Nu	Nusselt number
p	pressure
q_i	turbulent heat flux in x_i-direction, $\overline{u_i' T'}$
q_v	volumetric heat source
Pr	Prandtl number, ν/κ
Ra_E	external Rayleigh number, $g\beta\,\Delta T D^3/(\nu\kappa)$
Ra_I	internal Rayleigh number, $g\beta q_v D^5/(\nu\kappa\lambda)$
t	time
T	temperature
ΔT	temperature difference
u_i	velocity component in x_i-direction
u_0	velocity scale, $(g\beta\,\Delta T_0 D)^{1/2}$
x_i	coordinates in horizontal $(i=1,2)$ and vertical $(i=3)$ direction
X_i	periodicity length in x_i-direction $(i=1,2)$

Greek

β	coefficient of thermal expansion
δ_{ij}	Kronecker delta
κ	thermal diffusivity
λ	thermal conductivity
ν	kinematic viscosity
ρ	density

Subscripts

bottom	lower wall
max	maximum
ref	reference value
rms	root-mean-square value
top	upper wall
W	wall
0	initial value

Superscripts

$\overline{(\ )}$	time average
$(\ )'$	fluctuating component with respect to $\overline{(\ )}$
$\langle\ \rangle$	ensemble average over $x_1 - x_2$ plane and time
$(\ )''$	fluctuating component with respect to $\langle\ \rangle$

1. Introduction

To calculate turbulent flow and heat transfer by means of second-order statistical turbulence models, balance equations are solved for characteristic turbulent quantities such as the turbulence kinetic energy, its dissipation rate, the Reynolds stresses, the turbulent heat fluxes, and temperature variance. The balance equations actually solved are derived from analytical equations by introducing simplifications and model

* Corresponding author. E-mail: woerner@irs.fzk.de.

0142-727X/98/$19.00
PII: S0142-727X(97)10019-4

assumptions. In each analytical balance equation, terms can be classified in the categories: (1) rate of change, (2) convective transport, (3) production P, (4) sink S, and (5) diffusive transport D.

In fully developed natural convection where no mean flow through the channel is present, e.g. in the classical Rayleigh–Bénard convection in the fully turbulent regime, terms (1) and (2) drop out when averages are taken over long times. The balance equation for a general turbulent quantity ϕ then simplifies to

$$P_\phi + S_\phi + D_\phi = 0. \tag{1}$$

In a state of local equilibrium, the local production and sink of a quantity ϕ are in balance, thus $P_\phi = -S_\phi$ and $D_\phi = 0$. However, in many situations ϕ is mainly produced away from walls, while the sink term is largest near walls. Thus, there is no local equilibrium and the diffusive transport is important, as it redistributes ϕ across the flow domain. In such situations, accurate modelling of the turbulent part of diffusive transport $D_{\phi,\mathrm{turb}}$ is of special significance.

In this paper, we focus our attention on the balance equations for turbulence kinetic energy $k = \frac{1}{2}\overline{u_i' u_i'}$ and turbulent heat fluxes $q_i = \overline{u_i' T'}$. Using the normalisation introduced below, the turbulent diffusive transport is represented in non-dimensional variables by the correlations

$$D_{k,\mathrm{turb}} = -\frac{\partial}{\partial x_j}\left(\frac{1}{2}\overline{u_j' u_i' u_i'} + \overline{u_j' p'}\right) \tag{2}$$

and

$$D_{q_i,\mathrm{turb}} = -\frac{\partial}{\partial x_j}\left(\overline{u_i' u_j' T'} + \delta_{ij}\overline{T' p'}\right). \tag{3}$$

Thus, velocity and pressure fluctuations contribute to $D_{k,\mathrm{turb}}$, and velocity, pressure and temperature fluctuations to $D_{q_i,\mathrm{turb}}$.

Modelling the pressure transport is particularly difficult, because pressure fluctuations within a turbulent flow are one of the "Great Unmeasurables" (Bradshaw, 1994). Based on theoretical considerations, Lumley (1978) suggests to account for the pressure transport of k by

$$\overline{u_j' p'} = \frac{1}{5}\overline{u_j' u_i' u_i'}. \tag{4}$$

Mansour et al. (1988) use direct numerical simulation (DNS) data of forced turbulent channel flow to compute budgets for Reynolds stresses $\overline{u_i' u_j'}$. Besides the region very close to the wall, they find the diffusive transport due to pressure–velocity correlations indeed being smaller than that due to triple velocity correlations. Wörner and Grötzbach (1993a, b) performed a series of direct numerical simulations of Rayleigh–Bénard convection in various fluids. From their results it appears that in this special type of convection not the triple correlation but the pressure correlation is the dominant term, both in Eqs. (2) and (3). However, no physical explanation for this surprising result is given by the authors.

The objective of the present paper is twofold. First, we investigate whether the special relevance of diffusive transport by pressure fluctuations is a general feature of natural convection in horizontal fluid layers or not. Besides the Rayleigh–Bénard convection, we therefore analyse direct numerical simulations of another type of pure natural convection, this is the convection in a horizontal fluid layer which is internally heated by a volumetric heat source. As will be shown, the relative importance of pressure diffusion as compared to the triple correlation in this type of convection is much smaller than in the Rayleigh–Bénard case. The second objective is therefore to give a physical interpretation for the dominance of pressure correlations in turbulent diffusive transport in Rayleigh–Bénard convection.

2. DNS of internally heated convection

The natural convection in a horizontal fluid layer of height D which is internally heated by a homogeneously distributed volumetric heat source q_v is of interest in several geophysical and technical systems. An example is reactor safety analysis in case of a hypothetical core melt down. A literature survey on investigations of internally heated convection is given by Kulacki and Richards (1985) and Nourgaliev et al. (1997).

The important dimensionless groups which characterise the physical problem are the internal Rayleigh number $\mathrm{Ra_I} = g\beta q_v D^5/(\nu\kappa\lambda)$ and the Prandtl number $\mathrm{Pr} = \nu/\kappa$, where g = gravity, β = thermal expansion coefficient, ν = kinematic viscosity, κ = thermal diffusivity, and λ = thermal conductivity. In the present study, the fluid Prandtl number is $\mathrm{Pr} = 7$ and the internal Rayleigh number ranges between $10^5 \leqslant Ra_\mathrm{I} \leqslant 10^9$.

Another important dimensionless number is the Damköhler number $\mathrm{Da} = q_v D^2/(\lambda \Delta T_{\max})$, where $\Delta T_{\max}$ is the maximum temperature difference across the channel. As $\Delta T_{\max}$ is not known a priori for a given q_v, the same holds for Da. For fully developed convection, where q_v is completely removed across top and bottom wall, it follows by an energy balance that Da equals the sum of the Nusselt numbers, i.e. $\mathrm{Da} = \mathrm{Nu_{top}} + \mathrm{Nu_{bottom}}$. Other dependent dimensionless numbers are the Grashof number $\mathrm{Gr} = \mathrm{Ra_I}/(\mathrm{Pr} \times \mathrm{Da})$ and the external Rayleigh number $\mathrm{Ra_E} = \mathrm{Ra_I}/\mathrm{Da}$.

Numerical Model: The direct numerical simulations are performed with the TURBIT code (Grötzbach, 1987). It is based on a finite volume method and solves the complete time-dependent three-dimensional conservation equations of mass, momentum, and energy. The Boussinesq approximation is employed, and the equations are solved in dimensionless form. For normalisation the channel height D, the velocity $u_0 = (g\beta\,\Delta T_0 D)^{1/2}$, the pressure ρu_0^2, and temperature difference ΔT_0 are used. The latter is related to a guess for the Damköhler number $\mathrm{Da_0} = q_v D^2/(\lambda\,\Delta T_0)$, which needs to be specified at the start of a simulation. Using the summation convention, the governing equations are given for a Cartesian coordinate system by:

$$\frac{\partial u_j}{\partial x_j} = 0, \tag{5}$$

$$\frac{\partial u_i}{\partial t} + \frac{\partial (u_i u_j)}{\partial x_j} = -\frac{\partial p}{\partial x_i} + \frac{1}{\sqrt{\mathrm{Gr_0}}}\frac{\partial^2 u_i}{\partial x_j \partial x_j} - \delta_{i3}(T_{\mathrm{ref}} - T) \quad (i = 1,2,3), \tag{6}$$

$$\frac{\partial T}{\partial t} + \frac{\partial (T u_j)}{\partial x_j} = \frac{1}{\mathrm{Pr}\sqrt{\mathrm{Gr_0}}}\left(\frac{\partial^2 T}{\partial x_j \partial x_j} + \mathrm{Da_0}\right). \tag{7}$$

The flow geometry and coordinate system of the horizontal channel are shown in Fig. 1. The boundary conditions used are rigid upper and lower horizontal walls at $x_3 = 0$ and $x_3 = 1$, respectively. For the simulations of the internally heated layer, both walls are isothermal and have equal temperature. In the horizontal directions $x_{1,2}$ periodic boundary conditions with periodicity lengths $X_{1,2}$ are applied. From an experimental point of view, this corresponds to the convection occuring in a container with large aspect-ratio.

Eqs. (5)–(7) are also valid for the Rayleigh–Bénard convection. Since in this case there is no heat generation in the fluid, q_v and Da_0 are zero. The temperature difference ΔT_0 is that one between heated lower and cooled upper isothermal wall: $\Delta T_0 = \Delta T_{\max} = T_{\mathrm{Wall,bottom}} - T_{\mathrm{Wall,top}}$.

In Table 1 we give the parameters and grid data of the simulations for the internally heated convection and for a recently refined simulation of Rayleigh–Bénard convection in air ($\mathrm{Pr} = 0.71,\ \mathrm{Ra_E} = 630,000$) (Wörner and Grötzbach, 1997).

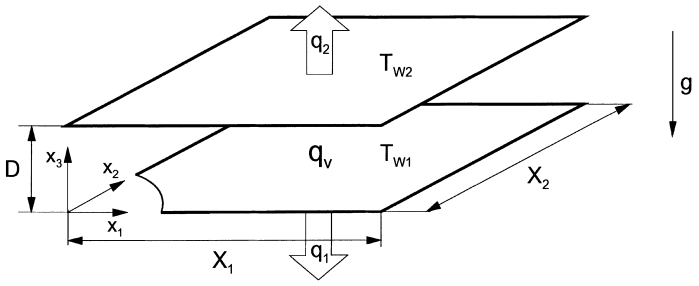

Fig. 1. Computational domain and coordinate system.

Table 1
Parameter and grid data of the simulations

Pr	Ra_I	$X_{1,2}$	$\Delta x_{1,2}$	$\Delta x_{3W,bottom}$	$\Delta x_{3,max}$	$\Delta x_{3W,top}$	N_1	N_2	N_3
	10^5	6	0.1000	0.0370	0.069	0.0320	60	60	21
	5×10^5	6	0.0750	0.0250	0.064	0.0190	80	80	27
	10^6	5	0.0625	0.0231	0.054	0.0161	80	80	31
7	5×10^6	5	0.0500	0.0228	0.049	0.0115	100	100	35
	10^7	5	0.0417	0.0180	0.036	0.0092	128	128	39
	10^8	4	0.0250	0.0120	0.026	0.0057	160	160	55
	10^9	3	0.0150	0.0061	0.019	0.0024	200	200	80
	Ra_E								
0.71	630,000	7.92	0.0396	0.0050	0.037	0.0050	200	200	49

$\Delta x_{1,2}$ = horizontal mesh widths (equidistant spacing), Δx_3 = vertical mesh widths (non-equidistant spacing, W = wall), $N_{1,2,3}$ = number of mesh cells.

We carefully ensured that the grids resolve the largest scales of convection and the smallest scales of turbulence and thus meet these indispensible requirements of the DNS method.

Verification: To verify the numerical results for the internally heated convection, the computed Nusselt numbers at top and bottom wall are compared with the experimental correlations of Jahn (1975) and Kulacki and Goldstein (1972), see Fig. 2. Besides the simulation with $Ra_I = 10^9$, where the Nusselt number at the lower wall in the computation is little too high as compared to the correlation of Jahn (1975), a very good agreement is achieved for the total heat transfer. For a more detailed verification of the simulations with $Ra_I = 10^6$ and $Ra_I = 10^7$ we refer to Wörner et al. (1997). There, we also discuss the patterns and dynamics of the convection, whereas

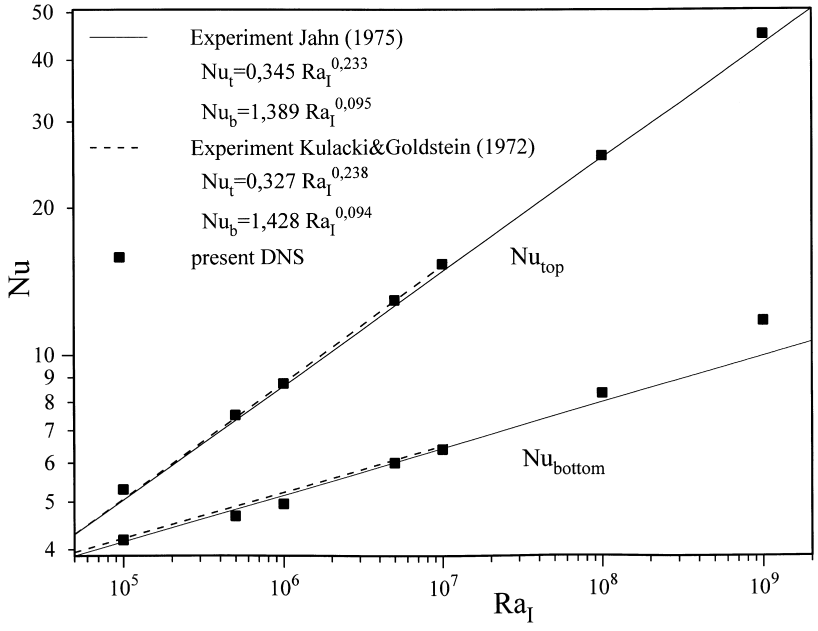

Fig. 2. Comparison of computed Nusselt numbers at top and bottom wall with experimental correlations for internally heated convection.

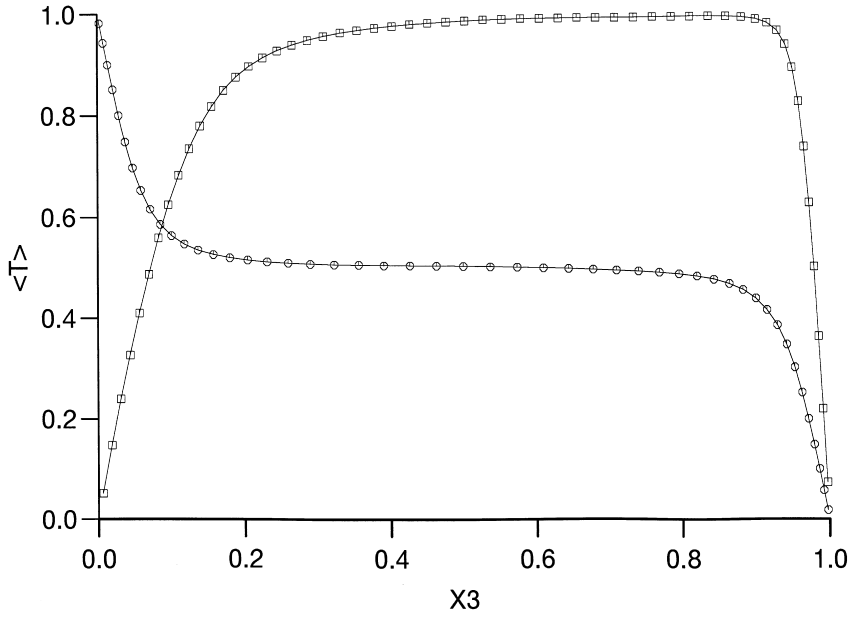

Fig. 3. Vertical profile of mean temperature $\langle T \rangle$. □: Internally heated convection ($Ra_I = 10^8$), ○: Rayleigh–Bénard convection ($Ra_E = 630{,}000$).

the present paper is limited to the analysis of turbulent diffusive transport of k and $\overline{u_3' T'}$.

3. Results for $D_{k,\mathrm{turb}}$ and $D_{q3,\mathrm{turb}}$

Case selection: For analysis of turbulent diffusive transport of k and $\overline{u_3' T'}$ we focus for the internally heated layer on the simulation with $Ra_I = 10^8$. The Grashof number is about 407,000 and thus is comparable to the Rayleigh–Bénard case, where $Gr \approx 887{,}000$. The Grashof number is the relevant dimensionless number in the momentum Eq. (6). As Gr is of similar magnitude in both simulations, the turbulence intensity and thus velocity and pressure fields should be comparable, too. In the dimensionless energy Eq. (7), the relevant parameter is the Boussinesq number $Bo = Pr^2 Gr$. In the simulation with $Ra_I = 10^8$ the value is $Bo \approx 2 \times 10^7$. This is about 50 times higher than in the Rayleigh–Bénard case, where $Bo \approx 447{,}000$. Thus, for the statistics of the temperature fields in both simulations we can not expect similarity.

Evaluation of statistical data: Statistical quantities are evaluated from the DNS data by ensemble averaging over horizontal planes and additional time averaging. This procedure results in vertical profiles of averaged quantities and is indicated by angled brackets, whereas the overbar denotes the conventional time averaging. Fluctuations with respect to $\langle \Phi \rangle$

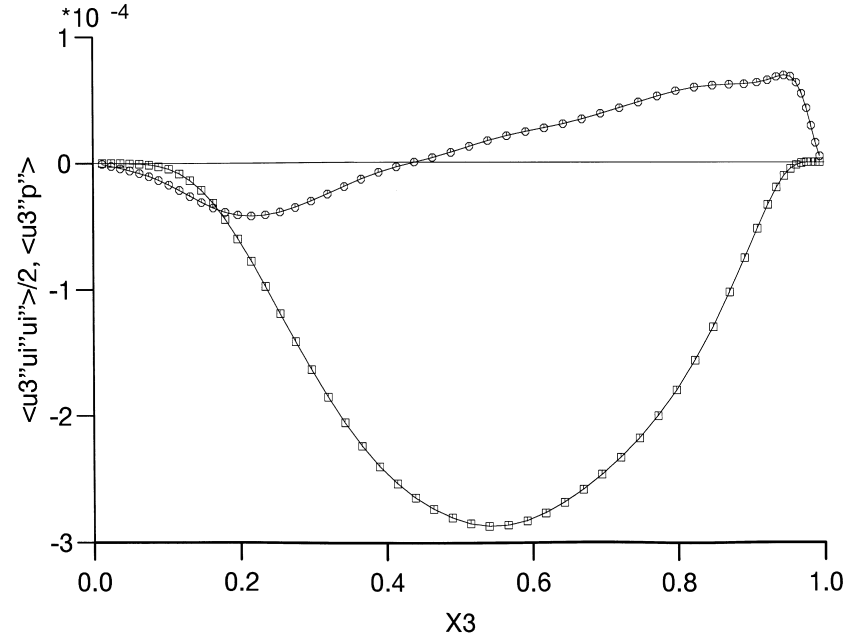

Fig. 4. Internally heated convection ($Ra_I = 10^8$). □: $\langle u_3'' u_i'' u_i'' \rangle / 2$, ○: $\langle u_3'' p'' \rangle$.

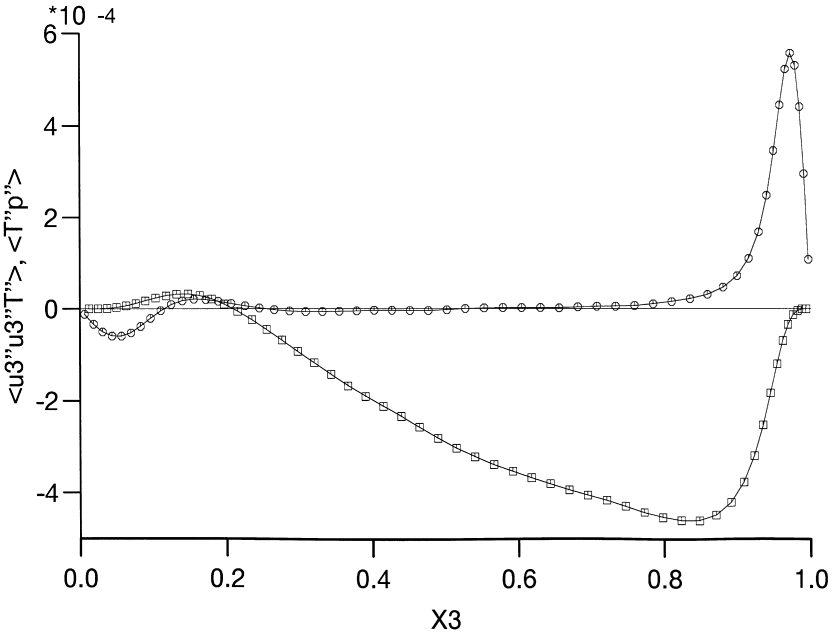

Fig. 5. Internally heated convection ($Ra_I = 10^8$). □: $\langle u_3'' u_3'' T'' \rangle$, ○: $\langle T'' p'' \rangle$.

are denoted by Φ'', and fluctuations with respect to Φ by Φ'. For the geometries and boundary conditions used in the present DNS, statistical data are homogeneous with respect to the horizontal directions. Therefore, for fully developed turbulent flow both types of averages should be equivalent.

In Fig. 3 we show evaluated profiles of mean temperature $\langle T \rangle$. The core region is almost isothermal, both, for the internally heated convection and for the Rayleigh–Bénard convection. In the Rayleigh–Bénard convection, both boundary layers near top and bottom wall are stratified thermally unstable. For the internally heated layer, there is a thin thermally unstable stratified boundary layer near the top wall and a thicker stably stratified one near the bottom wall.

Internally heated fluid layer: In Fig. 4 we show vertical profiles of the correlations $\langle u_3'' u_i'' u_i'' \rangle/2$ and $\langle u_3'' p'' \rangle$, which cause according to Eq. (2) diffusive transport of k in vertical direction. With exception of the regions near bottom and top wall, the absolute value of the triple correlation of velocity fluctuations exceeds that of the pressure correlation. The same holds for the absolute values of the vertical gradient of both correlations.

Fig. 5 gives profiles of correlations $\langle T'' p'' \rangle$ and $\langle u_3'' u_3'' T'' \rangle$, which contribute to turbulent diffusive transport of vertical turbulent heat flux. In natural convection, fluctuations of temperature and vertical velocity are closely related, since the first ones induce buoyancy forces which drive the vertical motion. Thus, one should expect that the profiles of triple correlation and pressure correlation, respectively, in Figs. 4 and 5 are similar. While this is partly true from a qualitative point of view, substantial differences are identified, too. Fig. 5 shows that in the centre of the layer $\langle T'' p'' \rangle$ is almost zero, whereas the triple correlation obeys an almost constant spatial gradient. Thus, in the centre of the layer diffusive transport of $\overline{u_3' T'}$ is only due to the triple correlation. At the edges of the thermal boundary layers $\langle T'' p'' \rangle$ shows peaks. Especially the one close to the upper wall is very sharp, indicating considerable pressure transport.

A comparison of the correlations given in Figs. 4 and 5 for $Ra_I = 10^8$ with those obtained for $Ra_I = 10^9$, not shown here, reveals no major influence of the increase of the internal Rayleigh number. In accordance with the thinner boundary layers, for $Ra_I = 10^9$ only a sharpening and shift of the peaks in the profile of $\langle T'' p'' \rangle$ towards the walls is observed.

Rayleigh–Bénard convection in air: As discussed in Section 1, from results of DNS of Rayleigh–Bénard convection in air and sodium at different Rayleigh numbers it is found that the pressure correlation represents the dominant turbulent transport term (Wörner and Grötzbach, 1993a, b). See e.g. Fig. 6, where profiles of $\langle u_3'' u_i'' u_i'' \rangle/2$ and $\langle u_3'' p'' \rangle$ are given for Rayleigh–Bénard convection in air. Furthermore, a remarkable similarity between both pressure correlations and both triple correlations in Eqs. (2) and (3) is found. Compare $\langle u_3'' p'' \rangle$ in Fig. 6 with $\langle T'' p'' \rangle$ in Fig. 7, and $\langle u_3'' u_i'' u_i'' \rangle/2$ in Fig. 6 with $\langle u_3'' u_3'' T'' \rangle$ in Fig. 7, respectively. For the triple correlations the similarity is striking, while the peaks in the profile of $\langle T'' p'' \rangle$ are more pronounced than in the profile of $\langle u_3'' p'' \rangle$.

Thus, we find that in the Rayleigh–Bénard convection the turbulent diffusive transport of k and $\overline{u_3' T'}$ is mainly due to pressure transport, whereas in the internally heated convection the pressure transport is only of minor importance and the triple correlations in Eqs. (2) and (3) represent the dominant terms. This result is quite surprising, since both physical problems under investigation are pure natural convection flows, taking place in the same geometrical configuration, and having quite similar boundary conditions. Therefore, in Section 4 we try to illuminate this phenomenon by analysing the transport mechanisms occuring in both convection layers.

4. Mechanisms of pressure transport

Rayleigh–Bénard convection in air: To illustrate the mechanism of heat transfer and the dynamics of Rayleigh–Bénard convection in air (see also Grötzbach, 1995), we show in Fig. 8 the instantaneous isosurface for a dimensionless temperature value of $T = 0.7$ (bottom wall: $T = 1$, upper wall: $T = 0$). The color code is for vertical velocity (red: upward flow; green: $u_3 \approx 0$; blue: downward flow). Hot fluid rises in plumes from the heated lower to the cooled upper wall. Near the lower wall the upward velocity of a rising hot plume is initially low. In the core region, it is accelerated by buoyancy forces and eventually penetrates the boundary layer at the upper wall with high kinetic energy. As Fig. 8 shows, the plumes are concentrated in a few regions. In the boundary layer, these regions are con-

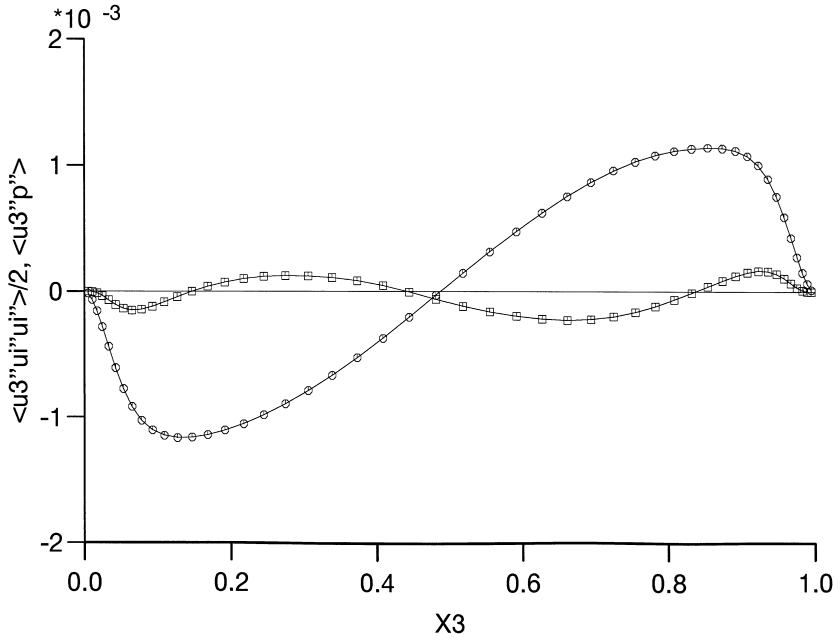

Fig. 6. Rayleigh–Bénard convection. □: $\langle u_3'' u_i'' u_i'' \rangle / 2$, ○: $\langle u_3'' p'' \rangle$.

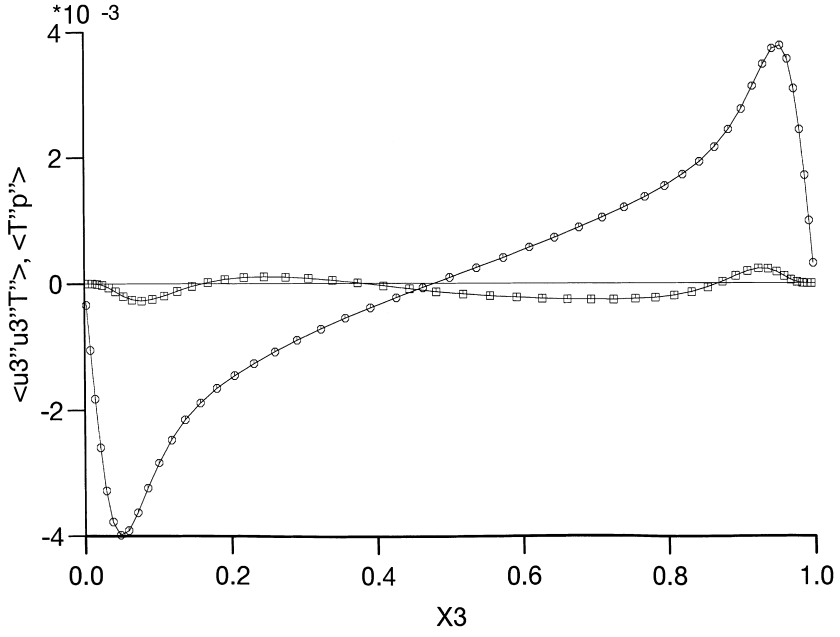

Fig. 7. Rayleigh–Bénard convection. □: $\langle u_3'' u_3'' T'' \rangle$, ○: $\langle T'' p'' \rangle$.

nected by thin spoke patterns formed by slowly upward moving fluid. The dynamics of the flow involves two time scales. The generation and rise of plumes and the horizontal translation of spokes are fast processes, while a horizontal translation of the areas with concentrated plumes occurs only on a much larger timescale.

In Fig. 9 we give a visualisation of the local value of correlation $u_3'' p''$ in plane $x_3 = 0.852$. From comparison of Figs. 8 and 9 we find that near the top wall high positive values of $u_3'' p''$ occur at locations where hot plumes rise and penetrate the boundary layer at the upper wall. At such a location, the local values of u_3'' and T'' are positive. Since the vertical velocity of the rising plume is retarded as it approaches the upper wall, the local pressure increases, i.e. $p'' > 0$. Thus, the correlations $u_3'' p''$ and $T'' p''$ take locally high positive values. Averaging of $u_3'' p''$ over the horizontal plane results in $\langle u_3'' p'' \rangle > 0$ and also $\langle T'' p'' \rangle > 0$ in the upper half of the channel (see Figs. 6 and 7). For the lower half of the channel, where cold plumes released from the top wall penetrate the boundary layer at the lower wall, the argumentation leading to $\langle u_3'' p'' \rangle < 0$ and $\langle T_3'' p'' \rangle < 0$ is equivalent.

Internally heated convection: The dynamics of convection in an internally heated fluid layer is as well similar to that in Rayleigh–Bénard convection as it is different, too. Similar, because in both configurations there is an unstable thermal stratification at the top wall. This causes the Rayleigh–Taylor instabil-

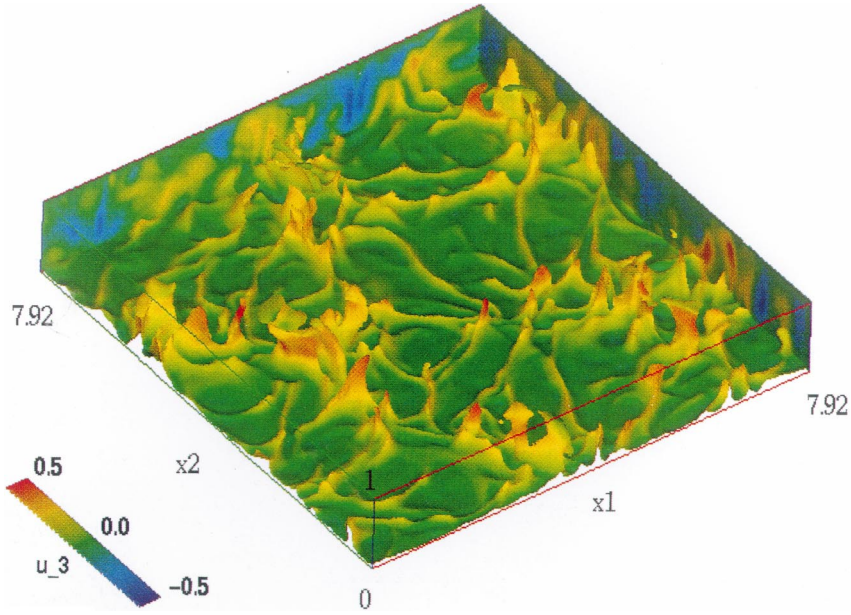

Fig. 8. Rayleigh–Bénard convection. Isosurface for instantaneous temperature $T = 0.7$ and color code for vertical velocity u_3.

ity to generate cold plumes which leave the upper wall. In the Rayleigh–Bénard case, also the boundary layer at the lower wall is stratified thermally unstable and plumes of warm fluid rise and finally reach the upper wall. By means of these plumes, which form at one boundary layer and penetrate the one at the opposite wall with high kinetic energy, there is strong interaction between both near wall regions. In contrast, in the internally heated convection the thermal stratification of the quite thick boundary layer at the lower wall is stable (see Fig. 3). The fluid in the lower part of the channel is therefore almost motionless and no rising plumes exist.

A detailed analysis of the present DNS data regarding the patterns and dynamics of the internally heated layer at the various Rayleigh numbers Ra_I can be found in Wörner et al. (1997). In this paper, we discuss only results for $Ra_I = 10^8$. The visualisation of the instantaneous temperature isovalue $T = 0.9$ in Fig. 10 shows a network of irregular cells. This characteristic pattern is well known and has been found in the experiments of Jahn (1975) as well as in the direct numerical simulations of Grötzbach (1987) for $Ra_I = 4 \times 10^6$. The lateral boundaries of the irregular cells are formed by thin vertical sheets of fast downward moving fluid (see color code for u_3 in Fig. 10), while in the inner region of the cells the motion is slow. In the temporal development, small cells contract and finally disappear. In the middle of large cells new plumes are generated due to the Rayleigh–Taylor instability. These cause new sheets to form, which eventually divide the large cell into two or more smaller ones.

As discussed in the previous section, the individual contribution of pressure transport to turbulent diffusion of k and

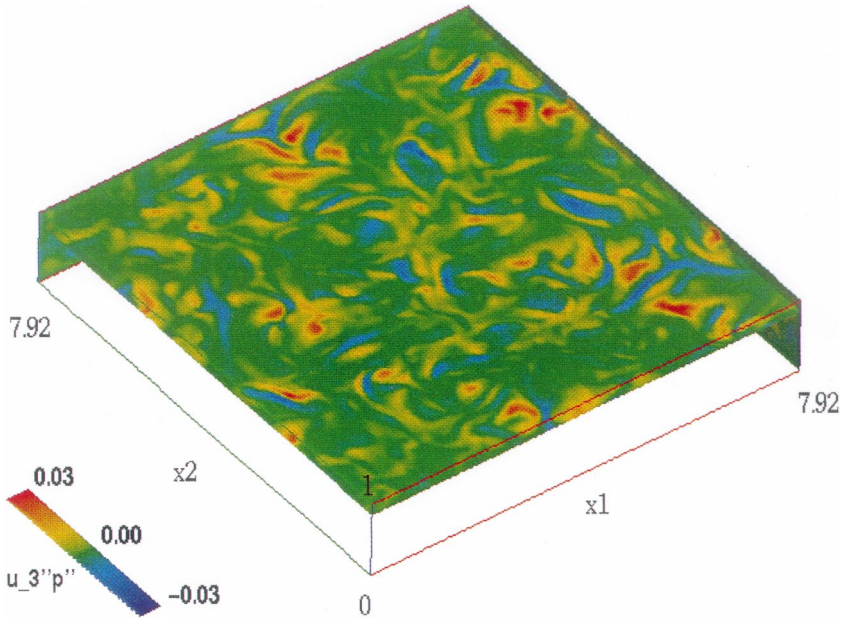

Fig. 9. Rayleigh–Bénard convection. Instantaneous local values of $u_3''p''$ in plane $x_3 = 0.852$.

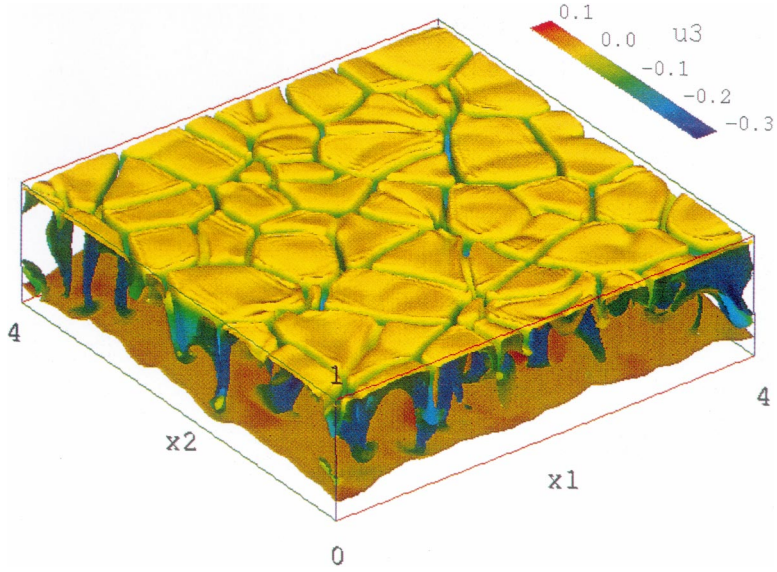

Fig. 10. Internally heated convection ($Ra_I = 10^8$). Isosurface for instantaneous temperature $T = 0.9$ and color code for vertical velocity u_3.

$\overline{u_3'T'}$ is much smaller in the internally heated convection than it is in the Rayleigh–Bénard case. The reason for this is that in the internally heated convection pressure fluctuations are much smaller than in Rayleigh–Bénard convection. This is indicated by a comparison of the root-mean-square values of pressure fluctuations. In the following, we give a physical explanation for this result. In the core region of the internally heated layer, cold plumes released from the top wall warm up. When such a descending plume reaches the edge of the thick boundary layer at the lower wall, its temperature is higher than that of the surrounding fluid. Thus, the orientation of the buoyancy force is no longer downward, but has switched to upward direction. Since now buoyant and viscous forces counteract the downward directed inertial one, the falling plumes are slowed down smoothly. They penetrate the boundary layer at the lower wall with much less kinetic energy than it is the case in the Rayleigh–Bénard convection. This explains why in the core region and in the lower part of the internally heated layer p_{rms} and correlations involving fluctuations of pressure are low. Since there are no plumes which rise from the bottom wall and penetrate the boundary layer at the upper wall, this statement holds for the whole layer.

An interesting result of the previous section is the profile of correlation $\langle T''p''\rangle$, given in Fig. 5. While in the core region the correlation is very small, it takes a high positive value in the thin thermal boundary layer at the upper wall. This sharp peak of $\langle T''p''\rangle$ results in considerable pressure transport of q_3. Fig. 11 gives a visualisation of the local instantaneous correlation $T''p''$ in plane $x_3 = 0.95$. From a comparison of Figs. 10 and 11 it follows, that the correlation $T''p''$ takes high positive values at the borders of the irregular cells, i.e. the vertical sheets with downward movement, and inside the cells. In the vertical sheets due to the slow acceleration of the cold downward falling fluid p'' is negative but small. However, because

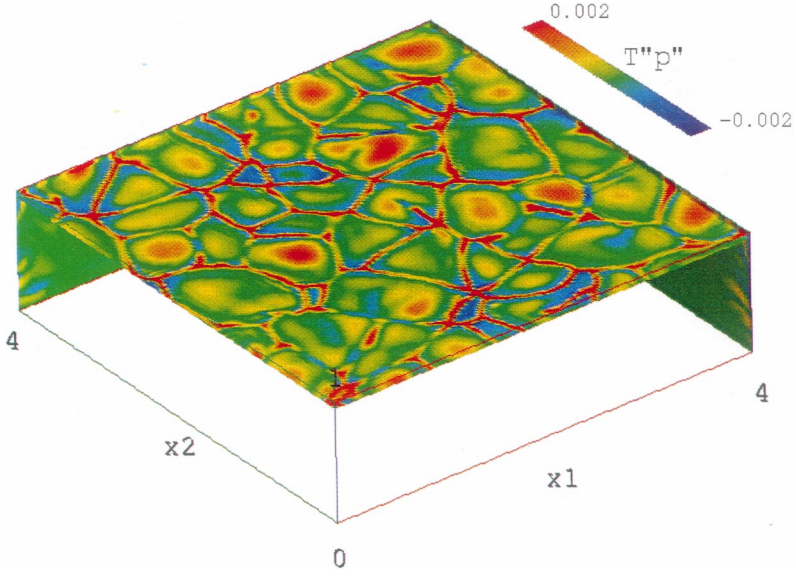

Fig. 11. Internally heated convection ($Ra_I = 10^8$). Instantaneous local values of $T''p''$ in plane $x_3 = 0.95$.

of the large gradient of $\langle T \rangle$ in the thin thermal boundary layer at the upper wall even a small downward displacement of fluid results in high negative values of T'' and thus in high positive values of local correlation $\langle T''p'' \rangle$.

5. Conclusions

Direct numerical simulation data of Rayleigh–Bénard convection in air ($Pr = 0.71$, $Ra_E = 630,000$) and of internally heated convection ($Pr = 7$, $Ra_I = 10^8$) are used to investigate turbulent diffusive transport of turbulence kinetic energy and vertical turbulent heat flux. For both quantities the turbulent diffusion consists of a pressure correlation and a triple correlation. In the statistical computation of turbulence these correlations are unknown and need to be modelled.

The analysis of the DNS data reveals that in the internally heated convection the major contribution to turbulent diffusion is due to the triple correlation, while in the Rayleigh–Bénard convection it is due to the pressure correlation. Thus, the dominance of pressure fluctuations in turbulent diffusive transport of turbulence kinetic energy and vertical turbulent heat flux, found in earlier numerical studies for the Rayleigh–Bénard problem, is not a general feature of natural convection in horizontal fluid layers. It appears that the importance and efficiency of pressure transport is closely linked to the flow mechanisms and to the dynamics of the convective layers. Namely in the Rayleigh–Bénard case, the efficient pressure transport of turbulence kinetic energy and vertical turbulent heat flux is related to intermittent coherent structures, i.e. plumes, with large kinetic energy.

In statistical turbulence models, closure assumptions are usually based on long-time averaged mean quantities (e.g. velocity or temperature). However, in turbulent Rayleigh–Bénard convection as well as in internally heated convection the long-time averaged mean velocity is zero, while on the time scale of the lifetime of coherent structures well defined mean values do exist. As shown above, an efficient transport of statistical turbulence quantities is combined with these coherent structures. Thus, for statistical computations of the flows under consideration it is essential to capture these structures. This seems to require full three-dimensional calculations as well as improved closure relations for turbulent diffusive transport which may not be based on long-time averaged mean quantities.

References

Bradshaw, P., 1994. Turbulence: The chief outstanding difficulty of our subject. Experiments in Fluids 16, 203–216.

Grötzbach, G., 1987. Direct numerical and large eddy simulation of turbulent channel flows. In: Cheremisinoff, N.P. (Ed.), Encyclopaedia of Fluid Mechanics, vol. 6. Gulf Publ., Houston, pp. 1337–1391.

Grötzbach, G., 1995. Direct numerical and large eddy simulation of turbulent heat transfer. In: Hanjalić, K., Pereira, J.C.F. (Eds.), Turbulence, Heat and Mass Transfer 1. Begell House, pp. 25–39.

Jahn, M., 1975. Holographische Untersuchung der freien Konvektion in einer Kernschmelze. Dissertation, TU Hannover.

Kulacki, F.A., Goldstein, R.J., 1972. Thermal convection in a horizontal fluid layer with uniform volumetric energy sources. J. Fluid Mech. 55, 271–287.

Kulacki, F.A., Richards, D.E., 1985. Natural convection in plane layers and cavities with volumetric energy sources. In: Kakac, S. Aung, W. Viskanta, R. (Eds.), Natural Convection: Fundamentals and Applications. Springer, Berlin, pp. 179–255.

Lumley, J.L., 1978. Computational modelling of turbulent flows. In: C.-S. Yih (Ed.), Advances in Applied Mechanics, vol. 18. Academic Press, New York, pp. 123–176.

Mansour, N.N., Kim, J., Moin, P., 1988. Reynolds-stress and dissipation rate budgets in a turbulent channel flow. J. Fluid Mech. 194, 15–44.

Nourgaliev, R.R., Dinh, T.N., Sehgal, B.R., 1997. Effect of Prandtl number on heat transfer characteristics in internally heated liquid pools with Rayleigh numbers up to 10^{12}, Nuclear Engineering and Design 169, 165–184.

Wörner, M., Grötzbach, G., 1993a. Analysis of diffusion of turbulent kinetic energy by direct numerical simulations of natural convection in liquid metals. Proceedings of NURETH-6, vol. 1. Grenoble, France, pp. 186-193.

Wörner, M., Grötzbach, G., 1993b. Turbulent heat flux balance for natural convection in air and sodium analysed by direct numerical simulations. Proceedings of the Fifth International Symposium on Refined Flow Modelling and Measurements. Paris, France, pp. 335–342.

Wörner, M., Grötzbach, G., 1997. DNS database of turbulent convection in horizontal fluid layers. http://hbksun 17.fzk.de:8080/IRS/eng/IRS3/TURBIT.DNS.database.html.

Wörner, M., Schmidt, M., Grötzbach, G., 1997. DNS of turbulence in an internally heated convective fluid layer and implications for statistical modelling. Journal of Hydraulic Research, 35, 773–797.